(Received 4 March 2026, Accepted 8 May 2026, Scheduled 1 July 2026)

CRLH-TL-Hilbert Structure Inspired Antenna Loaded with AMC Reflector for Wireless Applications

Marwa M. Ismail[1], Saif M. B. Alsabti[2], Raya A. Kamil[3], Mohammed A. D. Al-Obaidi[4], Bashar S. Bashar[5], Yaser A. Jassim[6], and Taha A. Elwi[7,*]

[1]*Department of Information and Communication Engineering, College of Information Engineering Al-Nahrain University, Jadriya, Baghdad, Iraq*
[2]*Technical College of Engineering, Al-Bayan University, Baghdad, Iraq*
[3]*Public Relations Department, College of Media Aliraqia University, Baghdad, Iraq*
[4]*Altinbaş University Esentepe, Şişli Büyükdere Cd. No.: 147 Beşiktaş/İstanbul 34349, Türkiye*
[5]*Department of Computer Engineering Techniques College of Engineering, University of Al Maarif, Al Anbar 31001, Iraq*
[6]*International Applied and Theoretical Research Center (IATRC), Baghdad Quarter, Iraq*
[7]*Department of Automation and Artificial Intelligence Engineering College of Information Engineering at Al-Nahrain University, Baghdad, Iraq*

ABSTRACT: High-gain reconfigurable antennas have become a crucial component of 5G systems. However, traditional Composite Right-Left-Hand Structure (CRLH) and Artificial Magnetic Conductor (AMC)-based designs suffer from high complexity, via losses, and complex biasing circuits. In this work, a CRLH transmission line integrated with a Hilbert Electromagnetic Band Gap (EBG) structure and a zero-phase AMC reflector is proposed for sub-6 GHz band. The proposed design integrates CRLH minimization, AMC gain enhancement, and Light-Dependent Resistor (LDR) bias-free reconfiguration within a unified low-complex framework. The design consists of 17-unit cells of a CRLH coupled to an EBG of Hilbert inclusions. An AMC reflector with zero phase shift is designed in the interested band to reduce back lobes and increase gain in forward direction. A maximum gain of 16 dBi was achieved at 5.5 GHz, and an increase of 4 dBi was achieved with the introduction of the AMC. An optical switch of LDRs controls antenna performance, where different scenarios are investigated to achieve reconfiguration and beam scanning. The antenna gain is highly affected by changing the LDR switching status; for example, a t5 GHz, the antenna gain varies between 9 dBi and 11 dBi. At 5.5 GHz, the gain varies between 18 dBi and 20 dBi. In addition, the antenna achieved a scan of $\mp 5^\circ$ with a consistent gain at 5 GHz by changing the LDR states. Therefore, the proposed antenna is an excellent candidate for direct amplitude modulation. Finally, the simulated results were validated through experimental measurements.

1. INTRODUCTION

Owing to the increased demand for wireless communication systems, it has become essential to develop adaptive, inexpensive antennas with high performance, including multi-band and good gain, specifically for 5G systems [1, 2]. Recently, different methods have emerged for designing miniature antennas using metamaterial (MTM) loadings [3]. MTM are manufactured using either a transmission line or resonance approach. The transmission line approach consists of a CRLH structure characterized by a combination of right-handed (RH) and left-handed (LH) transmission properties. In contrast, the resonant approach consists of split ring resonators (SRRs) and complementary split ring resonators (CSRRs) [4].

The transmission line structure is characterized by zero-order resonance, which is a very important feature of MTM antennas when the resonance of the antenna becomes distinct and independent of the length of the transmission line [5]. Nevertheless, the MTM compact design results in low gain, narrow bandwidth, low radiation efficiency, and high design complexity due to the use of vias, which restricts the use of metamaterials in various wireless applications [6]. To overcome these limitations, various methods have been used, including EBG, Perfect Electric Conductor (PEC), AMC reflector, and MTM substrate loadings [7]. However, these multi-layer antennas have large sizes, narrow bandwidths, low efficiencies, and low gains. In addition, the via complicates the antenna's fabrication process [8–10]. Hence, these antennas are unsuitable for applications that require high efficiency with lower complexity.

In this work, an AMC reflector was combined with a CRLH-TL-based antenna to enhance gain, radiation efficiency, and beamwidth for 5G systems. The use of AMC has attracted increased interest in recent years due to its distinctive characteristics [11]. In the context of AMC-based CRLH antennas, Ali et al. [12] presented a dual-band antenna that uses a CRLH coupled with an AMC, achieving a significant improvement in gain at operating frequencies. The radiator antenna, designed with the proposed AMC-MS (metasurface), achieves the gain enhancement of 6.46 and 7.12 dBi for the two frequency bands centered at 3.27 and 5.11 GHz, respectively. A heart-shaped antenna with a 3×3 AMC ground plane was designed [13]; in the

* Corresponding author: Taha Ahmed Elwi (taelwi82@gmail.com).

presence of an AMC, it achieves a peak gain of 5.86 dBi at the WiMAX band, representing a 225% increase in gain. Similarly, at the WLAN band, the antenna achieves a gain of 5.33 dBi, which represents a 141% increase in gain. A Coplanar Waveguide (CPW)-fed monopole antenna with an AMC structure was proposed [14], and dual-band operation was achieved and extended from 2.37 to 2.5 GHz and from 4.45 to 4.9 GHz, with a peak gain of 5 dBi and 7.5 dBi, respectively. A multi-band antenna supported by AMC was presented [15]. The proposed AMC unit cell comprises four metallic nested rings (FMNRs) and four lumped capacitors. The antenna with AMC achieves the gain improvement of 4.93, 5.92, 5.54, and 4.95 dB at frequencies of 2.45, 3.5, 4.6, and 5.8 GHz, respectively. This makes it appropriate for applications such as WLAN, WiMAX, and 5G mobile communication systems. A dual-band, dual-polarized antenna was proposed [16]. The antenna includes two components: dual-band dipole antennas with $\pm 45^{\circ}$ polarization and the proposed AMC reflector. The antenna operates within the frequency ranges of 2.31–2.61 GHz and 5.13–5.50 GHz. A 4×4 AMC reflector is utilized to achieve a suitable unidirectional radiation pattern. Gains of 7.24 dBi and 8.93 dBi are achieved in the low and high frequency bands, respectively. A wideband slotted patch antenna with resistive loading was suggested for use in ground-penetrating radar (GPR) applications [17]. The design is supported by an optimized reflector consisting of a periodic array of square-loop elements, improving the antenna's directivity and gain. It achieves a maximum gain of 7 dBi over a wide frequency range of 0.6 to 4.6 GHz. An antenna with a metamaterial-based planar monopole design has been suggested [18]. To achieve unidirectional radiation, a 5×5 artificial magnetic conductor (AMC) surface is employed as a back cavity. This surface is placed beneath the antenna at a height of $\lambda_o/12$ mm. The antenna achieves a maximum gain of 8 dBi in the lower frequency band (3.1–8.3 GHz) and upper frequency band (8.4–14 GHz), making it appropriate for wideband wireless applications. A linearly polarized antenna based on an AMC is proposed [19]. A 6×6 array of AMC is suggested to minimize the dimension of the dipole [20]. The proposed AMC unit includes a circular patch featuring four groups of symmetrical slots. An increase in the gain of 9.9 dBi is achieved, reducing the profile from 0.190λ to 0.120λ.

Unlike conventional AMC-based antennas reported in the literature, the proposed design introduces a unique integration of CRLH transmission line structures with Hilbert-based EBG inclusions, eliminating the need for vias and thereby reducing fabrication complexity and associated losses. In addition, the use of optical switching based on LDRs provides a bias-free reconfiguration mechanism, which is rarely explored in CRLH-AMC antenna systems. The novelty of the proposed design lies in the integration of a CRLH architecture and Hilbert curves with an AMC reflector within a single, low-complexity system, which achieves both enhanced gain and reduced losses. Traditional vias have been eliminated and replaced with a Hilbert architecture to achieve the desired inductive behavior while minimizing surface waves. Furthermore, optical LDR switches are employed for reconfiguration without the need for complex bias circuitry. Therefore, the main contributions of this work can be summarized as follows: A via-less CRLH structure using Hilbert inclusions for loss reduction, a high-gain AMC-backed configuration achieving up to 20 dBi, and a simple optical reconfiguration technique enabling frequency tuning and beam scanning without biasing circuits.

In this study, a CRLH-TL antenna structure loaded with an AMC reflector is proposed for 5G applications. The proposed design is constructed from an interdigital capacitor (C_{IDC}) coupled in parallel to a T-stub-inductor (L_{TS}) to realize gain-bandwidth product enhancement. To reduce the effect of via losses, Hilbert inclusions were introduced to the antenna back panel. The proposed antenna consists of 17 symmetrical T-shaped CRLH unit cells loaded with a third-order Hilbert curve structure and fed with an asymmetric coplanar waveguide feed structure. A 7×10 reflector array was placed in front of the proposed antenna to realize gain-bandwidth product enhancement. The proposed antenna with an AMC reflector realized a maximum gain of 20 dBi at 5.59 GHz with $S_{11} \leq -6$ dB.

2. PROPOSED ANTENNA GEOMETRY AND DESIGN

Figure 1 displays a schematic view and the fabricated model of the CRLH-TL-based antenna. The proposed antenna model consists of two layers. The 1st layer is the CRLH-TL antenna depicted in Figures 1(a)–(b), and the 2nd layer is the proposed AMC reflector used to improve the antenna performance as shown in Figure 1. The CRLH-TL was fabricated on a Taconic RF-43 substrate with a relative permittivity (ε_r) of 4.3, permeability (μ_r) of 1, thickness of 1.57 mm, and loss tangent ($\tan\delta$) of 0.0033.

2.1. CRLH-TL Antenna Design

The CRLH-TL antenna illustrated in Figure 1(a) is supplied with an asymmetric coplanar waveguide (CPW) feeding structure, where the dimensions of the ground plane differ on both sides of the CPW-feeding technique. The CRLH-TL antenna contains an interdigital capacitor and five fingers on each side, which represent the series capacitor, along with a T-stub inductor that represents a shunt inductor, combined to produce the component necessary for the left-handed nature of the CRLH structure. To further explain the electromagnetic behavior of the CRLH structure, the dispersion relation of the CRLH transmission line can be expressed as:

$$\beta(\omega) = \sqrt{(\omega^2 L_R C_R - 1)\left(\frac{1}{\omega^2 L_L C_L} - 1\right)} \qquad (1)$$

where L_R and C_R represent the right-handed inductance and capacitance; L_L and C_L correspond to the left-handed components of the structure; β is the phase constant; and ω is the angular frequency. This relation describes the propagation characteristics of the CRLH unit cell and explains the transition between left-handed and right-handed behaviors, which is essential for achieving compact size and enhanced performance.

To avoid the drawbacks associated with conventional CRLH transmission lines, the via element was replaced with a third-order Hilbert curve structure. In the original design, the ground plane introduces a capacitive effect, storing electromagnetic energy, while the vias provide an inductive effect to balance this

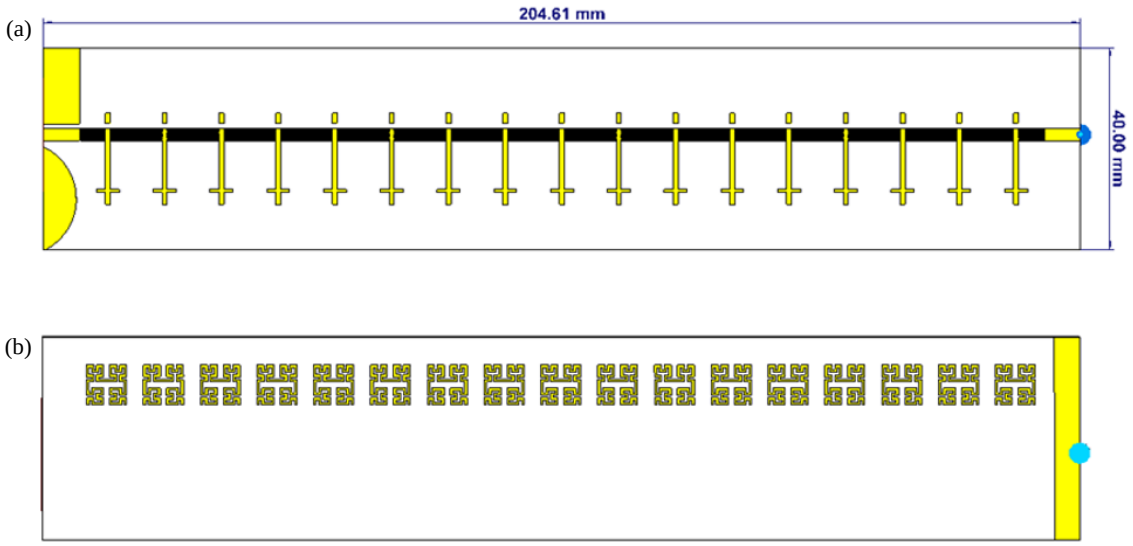

FIGURE 1. Antenna geometry. (a) CRLH-TL front view and (b) CRLH-TL back view.

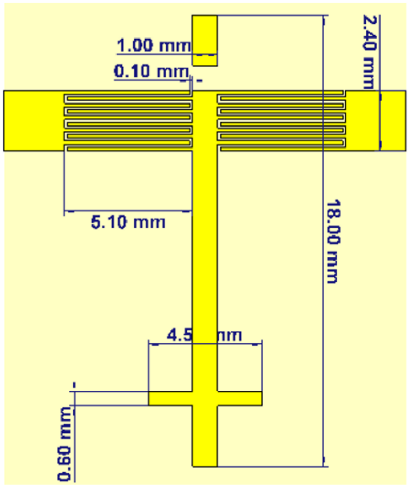

FIGURE 2. CRLH-TL unit cell dimensions.

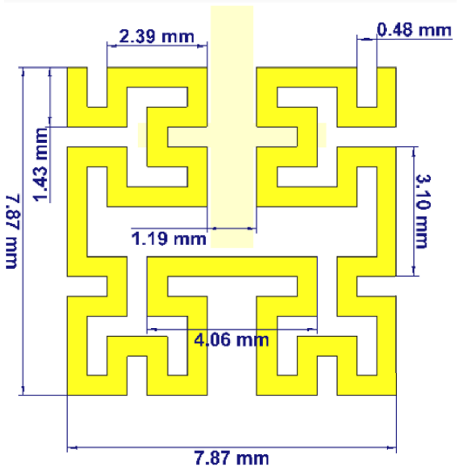

FIGURE 3. EBG structure.

capacitance. However, the use of vias increases conductivity losses, negatively impacting antenna gain. Therefore, the proposed Hilbert curve structure was adopted as an alternative solution to simulate the desired inductive behavior while minimizing losses and improving the overall radiative performance of the antenna.

The Hilbert curve structure, combined with the substrate, generates the parasitic effects required to realize the right-handed nature of the CRLH-structure, creating an antenna with higher gain and lower loss than the original design. The dimensions of the CRLH unit cell are shown in Figure 2. Furthermore, the ground plane represented by the copper layer acts as an antenna reflector, reflecting the signal with a phase opposite to that of the source wave. The term "source wave" generally refers to a wave that flows along the radiator. The "reflected wave", on the other hand, has a different phase compared to the source wave. This phase difference results in destructive interference with the source wave. Consequently, the main wave is completely canceled or significantly reduced, thereby decreasing the radiation efficiency. Consequently, the gain decreases owing to the mismatch caused by the cancellation of the field.

2.2. EBG Structure Antenna Design

EBG structures in the microwave and high-frequency ranges are periodic or semi-periodic structures generated by metallic impurities within magnetic or dielectric materials. They have been utilized for their unique characteristics in decreasing surface waves in many applications to enhance the overall performance. In this structure, a 17×1 array 3rd-order Hilbert curve structure is printed on the back surface of the substrate; their dimensions are adjusted to center the T-stub inductor with an area equal to $7.87 \times 7.87\,\text{mm}^2$, as shown in Figure 3.

In a classical EBG structure, a capacitive gap is generated between neighboring cells, which can be calculated using the following equation:

$$c = \frac{p\varepsilon_o(1+\varepsilon_r)}{\pi} \cosh^{-1}\left(\frac{p+g}{g}\right) \tag{2}$$

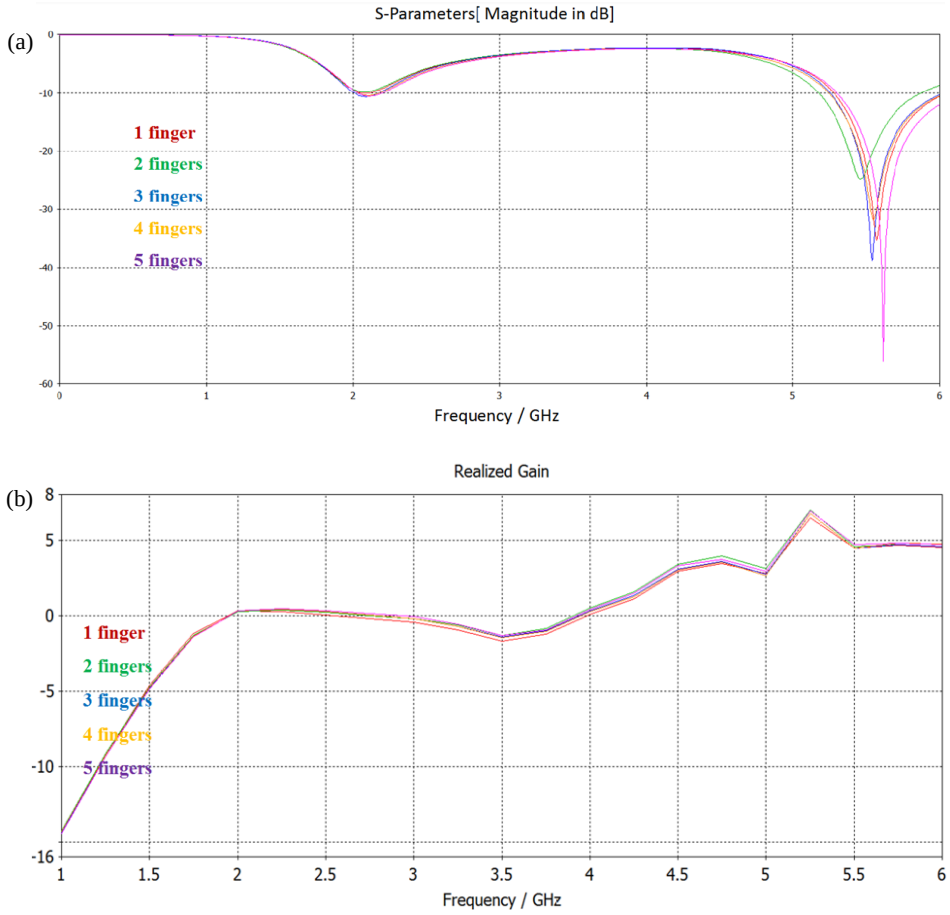

FIGURE 4. C_{IDC} effects. (a) S_{11} and (b) realized gain.

where p represents the width of the unit cell, g the gap between adjacent cells, ε_0 the permittivity of free space, and ε_r the relative permittivity of the substrate. EBG structures exhibit capacitance behavior and operate as a high-pass filter, allowing the transmission of high frequencies while suppressing low frequencies. The capacitive effect is symmetrical on both sides of the cell because the cell is balanced based on the length of the stub. The number and size of the cells were selected based on the EBG structural size, maximum antenna size, and manufacturing limitations. Therefore, the effect of the capacitive reactance of the neighboring cells has an equivalent effect on suppressing surface currents, as expressed by the following equation:

$$xc = \frac{1}{2\pi f c_{gap}} \tag{3}$$

where f is the operating frequency, and C_{gap} is the capacitance between adjacent EBG cells.

3. RESULTS AND PARAMETRIC STUDY

This section explains the antenna design process and the fundamental parameters for achieving the results. The design was analyzed and simulated using the Computer Simulation Technology Microwave Studio (CST MWS) tool based on the finite integration technique. The simulation and design procedure were partitioned into the following sections.

3.1. CRLH-Unit Cell Study and Stimulation

To clarify the effect of cell dimensions on the desired results, a detailed study was conducted for each of the following.

3.1.1. Inter Digital Capacitor Parametric Study

A detailed study was conducted on the effect of the number of fingers on antenna performance, where the number of fingers varied from 1 to 5, and the S_{11} and gain were calculated in each scenario. Figure 4(a) shows the effect of increasing the C_{IDC} fingers on the antenna impedance (S_{11}) by increasing the number of fingers. The impedance matching is improved, and the return loss is reduced due to the strong capacitive coupling inside the CRLH structure. This enhances the left-handed behavior of the CRLH structure and shifts the resonance toward the desired frequency with better impedance.

Figure 4(b) illustrates the effect of C_{IDC} fingers on the achieved gain. The gain increases slightly with an increasing number of fingers, as the improved current distribution reduces mismatch losses. Consequently, the antenna radiates more efficiently and achieves higher gain with the optimal five-finger configuration.

3.1.2. T-Stub Inductor Parametric Study

In this section, the dimensions of the inductance are changed to illustrate the effect of the dimensions on the design and results.

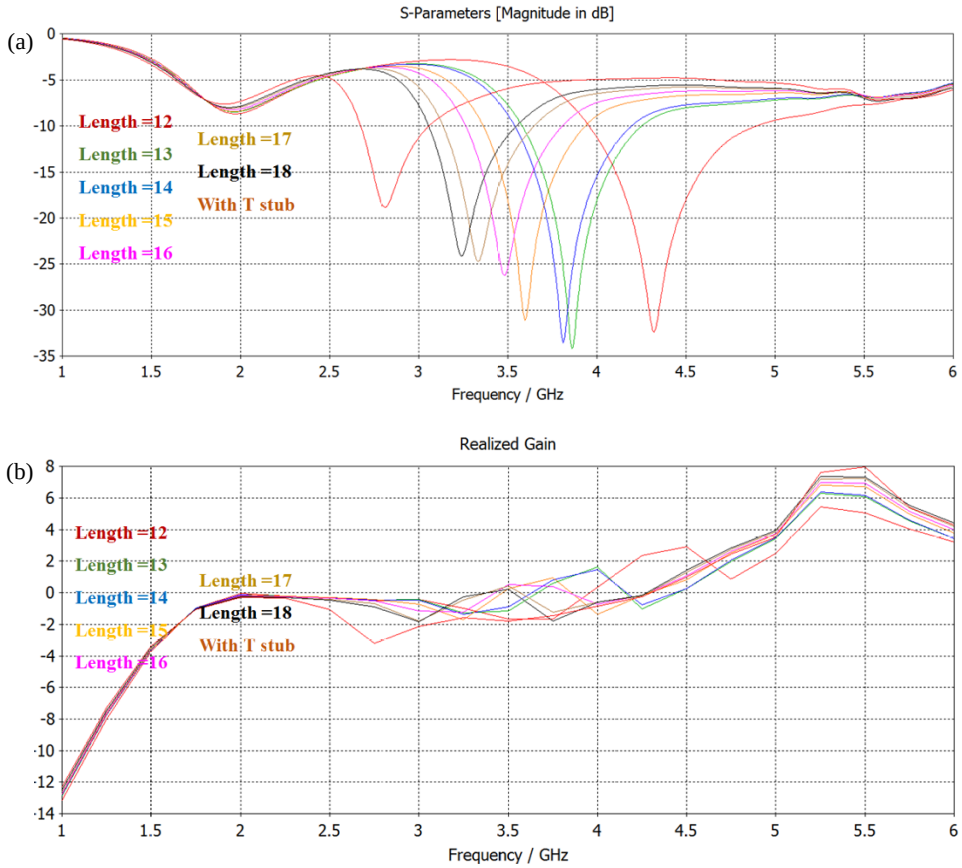

FIGURE 5. T_{SI} effects. (a) S_{11} and (b) realized gain.

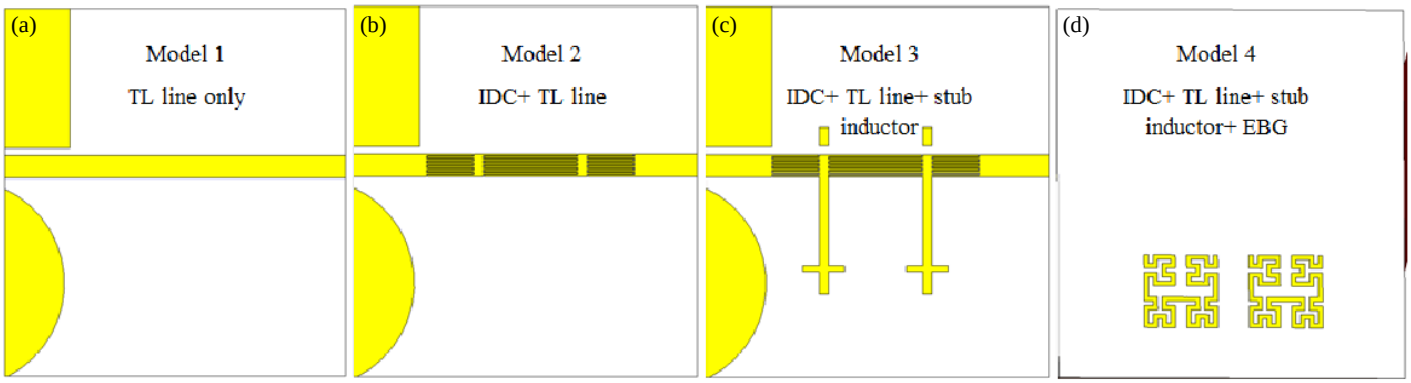

FIGURE 6. The CRLH geometrical details. (a) Model 1, (b) Model 2, (c) Model 3, and (d) Model 4.

Figure 5(a) shows the effect of the inductor length on the realized gain. Specifically, when the inductor length is increased from 12 to 18 mm, the gain increases from 6.69 to 8.8 dBi at a frequency of 5.4 GHz. Additionally, the T-shaped component located at the inductor operates as a small patch that helps distribute the electric current with high energy. Consequently, the gain increases and reaches a maximum value of 9.5 dBi for 2-CRLH unit cells separated by slots.

Figure 5(b) illustrates the effect of the inductor length on reflection coefficient (S_{11}); increasing the stub length shifts the resonance frequency to the lower bands, while introducing the T-stub balances the capacitive effects, reducing losses and increasing reflection coefficient.

3.1.3. CRLH Geometrical Details Parametric Study

A parametric study was conducted by decomposing the unit cell geometry into four basic models. The first model represents the transmission line only; the second model represents the transmission line-based I_{DC} capacitor, and the third model represents the transmission line with I_{DC} and I_{SI}. In this design, the fourth model represents the CRLH unit cell with the Hilbert curve added to represent the effect of the EBG defects on the antenna performance. Finally, the CRLH unit cell was connected to a one-port transmission line, as shown in Figure 6.

Figure 7(a) illustrates the evolution of the reflection coefficient across the different model configurations. In Model 1, the

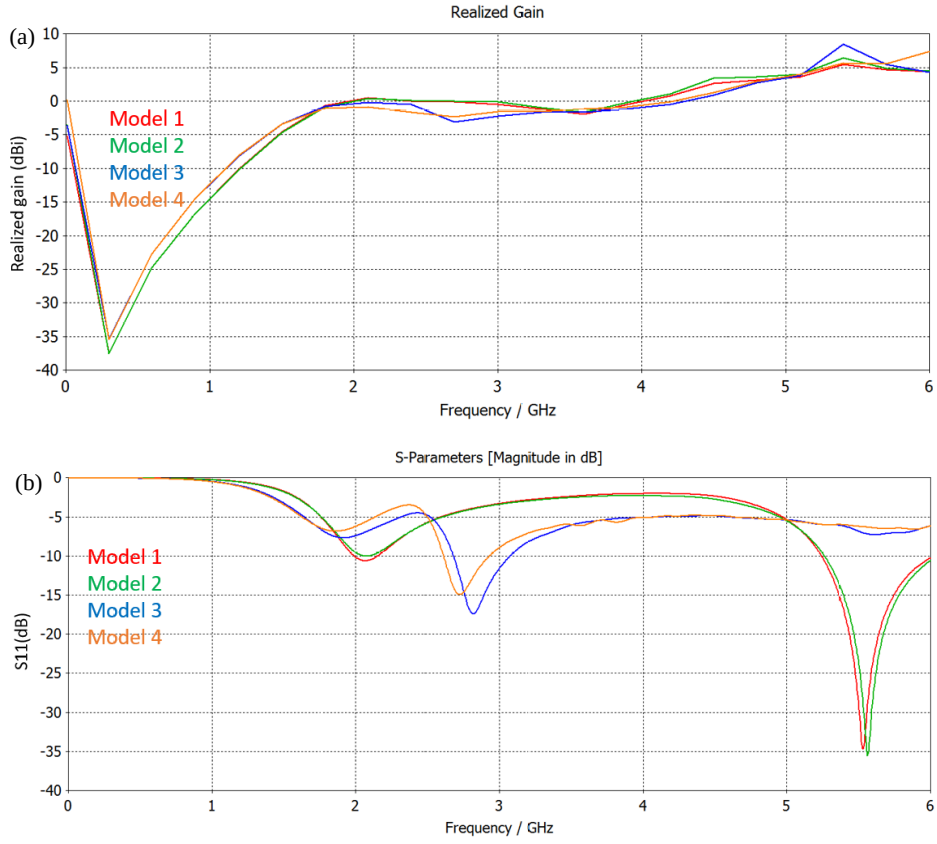

FIGURE 7. CRLH effects. (a) S_{11} and (b) realized gain.

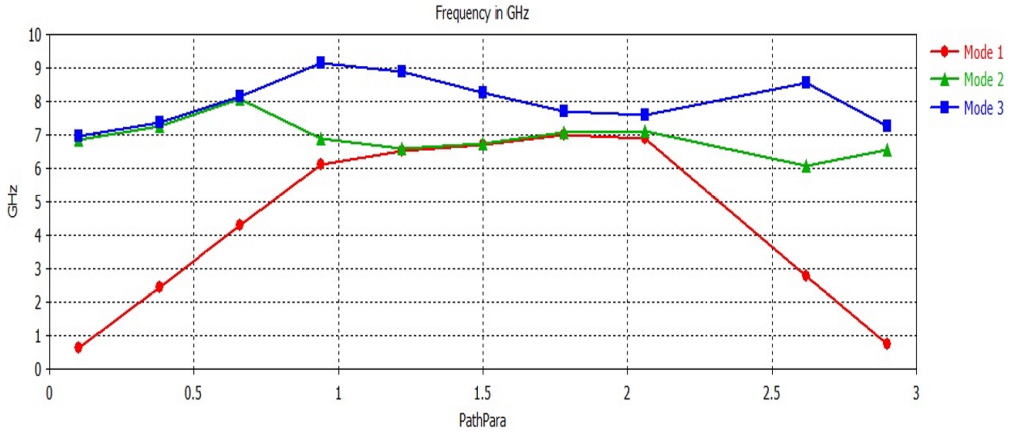

FIGURE 8. The dispersion diagram.

transmission line alone exhibits a weak resonance. The addition of a interdigital capacitor (CIDC) in Model 2 increases the capacitive effects and improves the left-hand response, resulting in a strong resonance. The introduction of a T-stub inductor balances the capacitive effects and shifts the resonance to lower bands. Finally, Model 4 with an EBG structure achieves the best match because it suppresses surface-wave losses, resulting in better stability.

Figure 7(b) illustrates the evolution of gain through different model configurations. In Model 1, the transmission line has low gain due to poor current distribution. Adding CIDC and a T-stub increases gain as the current distribution becomes more concentrated, which increases the efficiency of antenna radiation. Finally, Model 4 reduces surface-wave losses, resulting in better gain.

Figure 8 shows the properties of the CRLH unit cell proposed in Section 2.1, and the dispersion diagram is evaluated at various frequencies and angles for the three basic modes. The increasing slope indicated the right-hand region where the phase and group velocities are parallel; the saturation region indicates zero group velocity, and a stopband is created, while a decreasing slope indicated the left-handed region where the phase and group velocity are anti-parallel to each other.

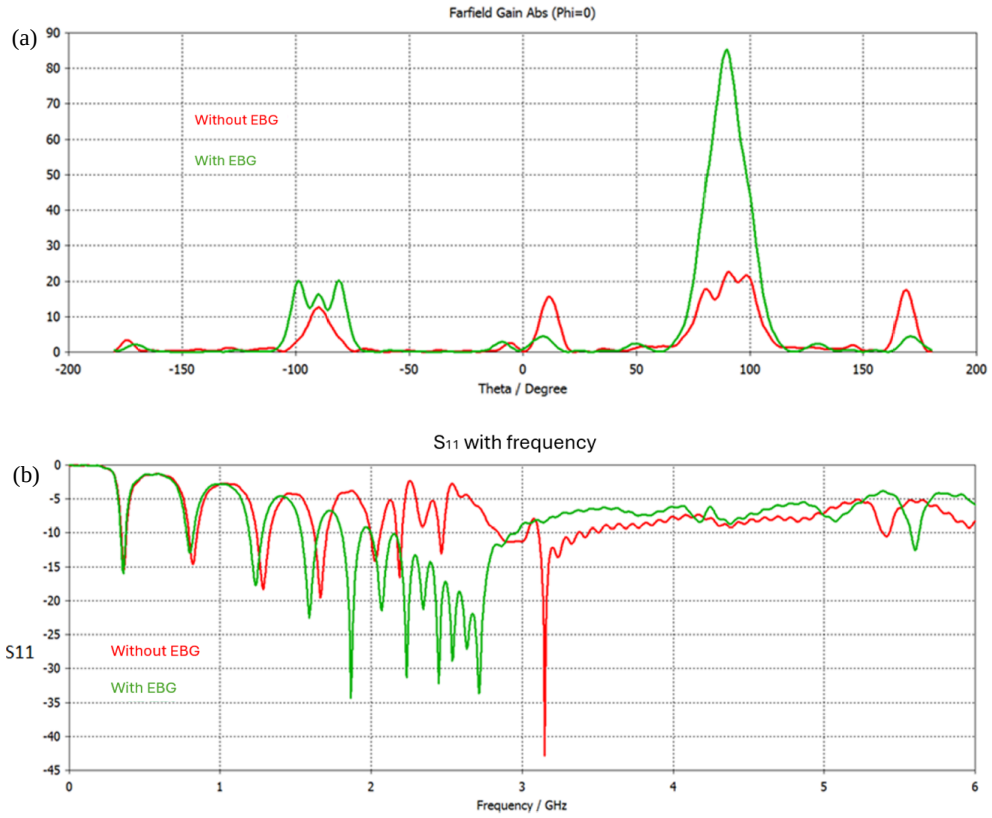

FIGURE 9. EBG effects. (a) S_{11} and (b) realized gain.

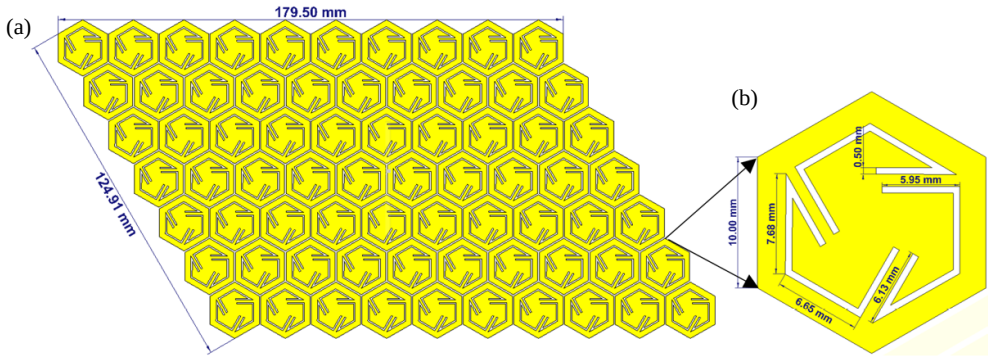

FIGURE 10. The proposed AMC reflector. (a) AMC layer and (b) unit-cell dimension.

3.2. Antenna Array with and without EBG Defects Parametric Study

This section comprehensively examines the effect of the MTM EBG structure on antenna performance. Two scenarios were considered, one with EBG defects and the other without. The gain and impedance bandwidths were studied and measured for each case. Figure 9(a) illustrates gain vs. EBG defects. The gain is significantly increased at 5.6 GHz, where the EBG reduces the surface-wave losses, resulting in better surface-current distribution and high radiation efficiency. Figure 9(b) shows the effect of EBG defects on impedance matching, and the Hilbert curve structure reduces losses and cooperates with the substrate to distribute the current with high efficiency, resulting in shifting the resonance frequency to higher frequencies with better matching and better performance.

4. REFLECTOR ANTENNA DESIGN

To provide a fair performance evaluation, the proposed design is analyzed under different configurations without a CRLH structure, without a Hilbert EBG, and without an AMC reflector. The results indicate that the CRLH structure contributes to miniaturization and impedance matching, while the Hilbert EBG reduces surface wave losses. The proposed AMC reflector significantly enhances the gain by providing in-phase reflection, resulting in an overall improvement of approximately 4 dB compared to the baseline design. A schematic illustration of the proposed reflector with a detailed view of the cell unit is shown in Figure 10, and the optimized values of the unit-cell dimensions are also presented. The reflector consists of 7×10 array elements arranged with a spacing equal to 0.5 mm and fills an area approximately equal to $179.5 \times 123.91\,\text{mm}^2$.

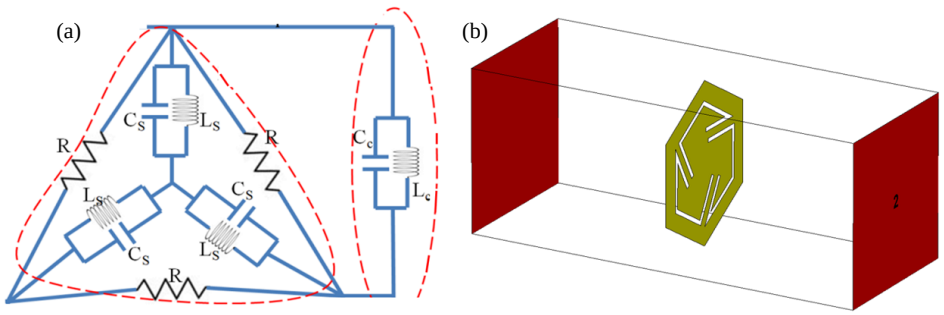

FIGURE 11. The proposed AMC structure. (a) Equivalent circuit model and (b) CST environment.

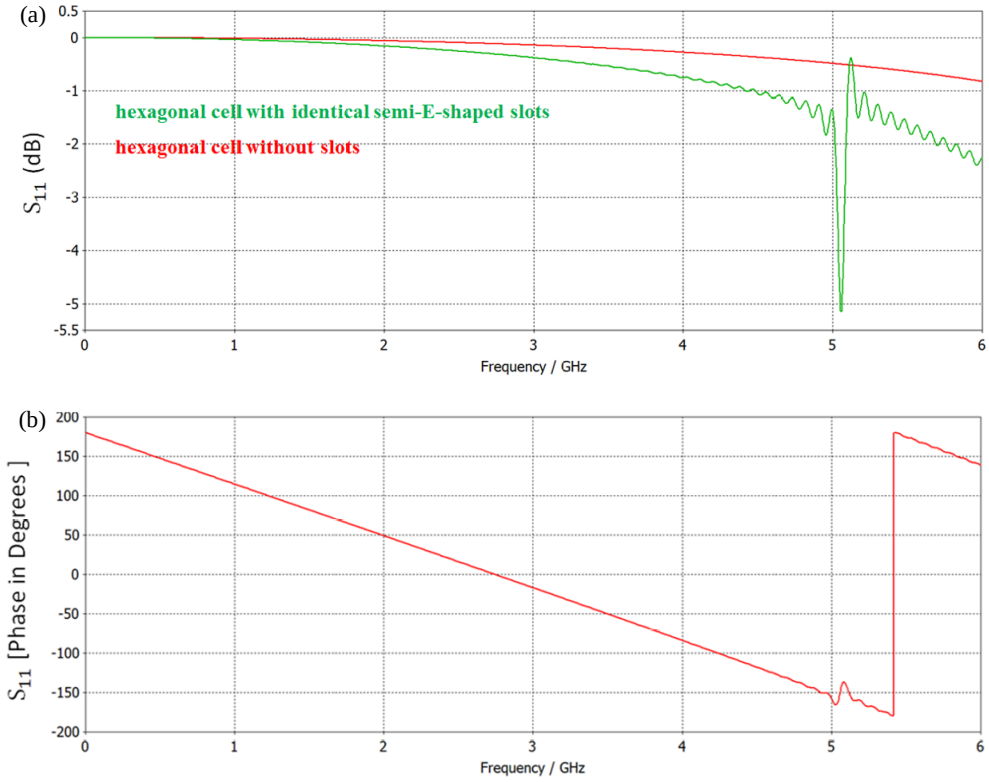

FIGURE 12. Simulated S_{11} spectra: (a) Magnitude and (b) phase.

4.1. Hexagonal Unit Cell Parameters

The proposed AMC unit cell equivalent circuit model is shown in Figure 11(a). Theoretically, the AMC unit cell consists of 3 slots arranged at an angle of 120° at the center of the patch. This arrangement induces a surface current motion that effectively enhances the radiation resonance frequency. The equivalent circuit representation can explain the resulting impact on antenna performance. The slot line effect is represented by the L_s loop. Thus, these slots are arranged as star-shaped connections within a delta branch. The proposed AMC coupling to the adjacent cells is determined by the parallel branches L_c and C_c. The proposed AMC simulation process was created and executed in the CST environment. The suggested AMC structure was presumed to be placed within a virtual waveguide with a square cross-sectional area. The waveguide is considered to have perfect electrical walls as its upper and lower boundaries, whereas its left and right boundaries are established as perfect magnetic walls. The remaining sides were equipped with two waveguide ports, generating excitement among the participants. In Figure 11(b), the first waveguide port is designated as the source, whereas the second port is fixed to monitor the output. To obtain the results for S_{11} and phase, they can be directly accessed numerically using this method.

When the proposed AMC is mounted inside a factitious waveguide, the cross-sectional cut is a square area that effectively mimics the plane wave incident. Figure 12(a) shows the S-parameters for the proposed AMC structure. Two scenarios are considered, one with star slots and the other without slots. The slots create a capacitive effect that balances the inductive effect and creates resonance at the band of interest.

Figure 12(b) shows the phase spectrum for the proposed AMC; the proposed AMC structure showed a zero-reflection phase at the band of interest, which is very useful for producing constructive interference that increases the surface current distribution and reduces losses, thereby enhancing the gain and bandwidth of the antenna design.

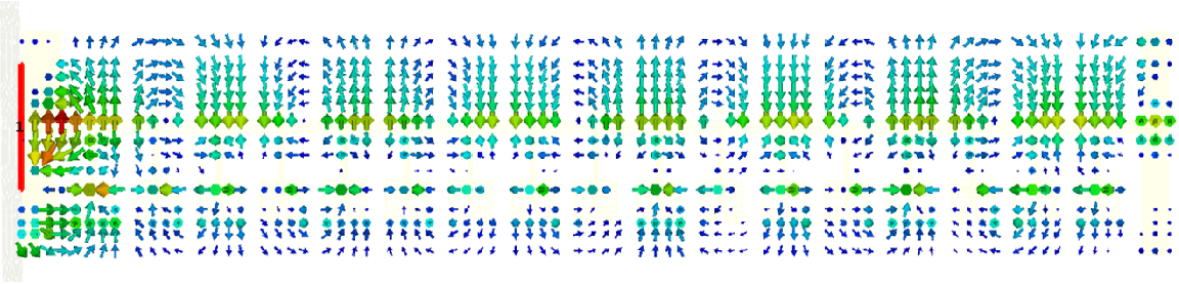

FIGURE 13. Surface current distribution of the antenna at 5.5 GHz.

The surface current distribution of the proposed antenna at 5.5 GHz is illustrated in Figure 13. It can be observed that the current is strongly concentrated along the CRLH transmission line elements, particularly around the interdigital capacitor and T-stub sections, indicating efficient excitation of the left-handed and right-handed modes. Moreover, the integration of the Hilbert EBG structure enhances current confinement by suppressing surface-wave propagation, leading to a more uniform current distribution along the radiator. This behavior reduces undesired energy leakage and improves radiation efficiency.

Additionally, the presence of the proposed AMC reflector plays a significant role in redirecting backward currents in the forward direction. The in-phase reflection property of the proposed AMC surface ensures constructive interference between the incident and reflected waves, resulting in stronger forward radiation and higher gain. It is also noticeable that the current intensity is higher near the feeding region and gradually decays along the antenna structure, which confirms proper power propagation across the 17-unit cells. This validates the effectiveness of the proposed design in achieving high gain and directive radiation performance.

4.2. AMC Study

A study was conducted on the array cells to demonstrate the impact of the proposed AMC array cells on antenna performance. First, the array cells were changed, and four cases were considered. The radiation field was evaluated in each case and compared. The suggested array size provides the highest gain with high impedance matching, as shown in Figure 14; consequently, an array of 7×10 cells was selected for the design. The proposed AMC surface exhibits a zero-reflection phase at the resonant frequency, which enables in-phase reflection of the incident wave, leading to constructive interference and enhanced radiation gain.

4.3. Frequency Reconfiguration and Beam Scanning

The optical switching mechanism is realized using Light Dependent Resistors (LDRs). In practice, the LDR elements are integrated within small gaps in the T-stub of each CRLH cell, allowing for current path control via lighting without the need for complex bias circuitry. The change in resistance between the on and off states modifies the effective electrical length of the antenna, thus enabling frequency reshaping and beam steering. Furthermore, the impact of these switches on radiation efficiency remains limited due to low losses and the absence of the need for additional power supply lines. From a practical standpoint, each LDR is soldered across a narrow gap in the conductive path, enabling direct control of the current flow as a function of the incident light intensity. Under illumination, the LDR exhibits a relatively low resistance (typically in the range of 100–500 Ω), effectively acting as a conductive path (ON state). In contrast, in the absence of light, its resistance increases to several mega-ohms, approximating an open circuit (OFF state). This transition allows a dynamic control of the antenna's effective electrical length, which directly leads to frequency reconfiguration and beam-steering capabilities.

Importantly, the integration of LDR-based switching introduces only marginal ohmic losses in the ON state, while negligible current flows in the OFF state. As a result, the overall radiation efficiency of the antenna is largely preserved, with only minimal degradation compared to the non-switching configuration. This demonstrates that the proposed approach is both practical and efficient for reconfigurable antenna applications. In addition, the optical control mechanism eliminates the need for DC biasing circuits, thereby reducing design complexity and minimizing parasitic effects typically associated with conventional electronic switches.

Table 1 shows the ability of the proposed system for frequency reconfiguration and gain control, which is essential for adaptive antennas in 5G systems. As listed in Table 1, different resonance frequencies can be achieved by modifying the optical switch (OS) states according to the input sequence, in addition to direct gain control, demonstrating the capability of the proposed antenna for direct antenna modulation.

This study compares LDR-based optical switching with conventional PIN diodes. Table 2 illustrates PIN diodes to highlight the effectiveness of the proposed approach. While PIN diodes offer a faster switching mechanism and better suitability for RF beamforming systems, they require complex DC bias circuits that introduce parasitic electromagnetic effects and increase manufacturing complexity. In contrast, the proposed LDR switching approach provides a bias-free, electromagnetically isolated, and low-complexity mechanism, making it highly attractive for integrated CRLH-AMC antenna systems.

Figure 15(a) shows the effect of the OS on impedance matching; multiple resonances are obtained by changing the OS configuration. It is observed that lower resonant frequencies occur in the ON state due to short-circuit behavior, and this dominates the design for systems with multiple applications, such as IoT and 5G systems.

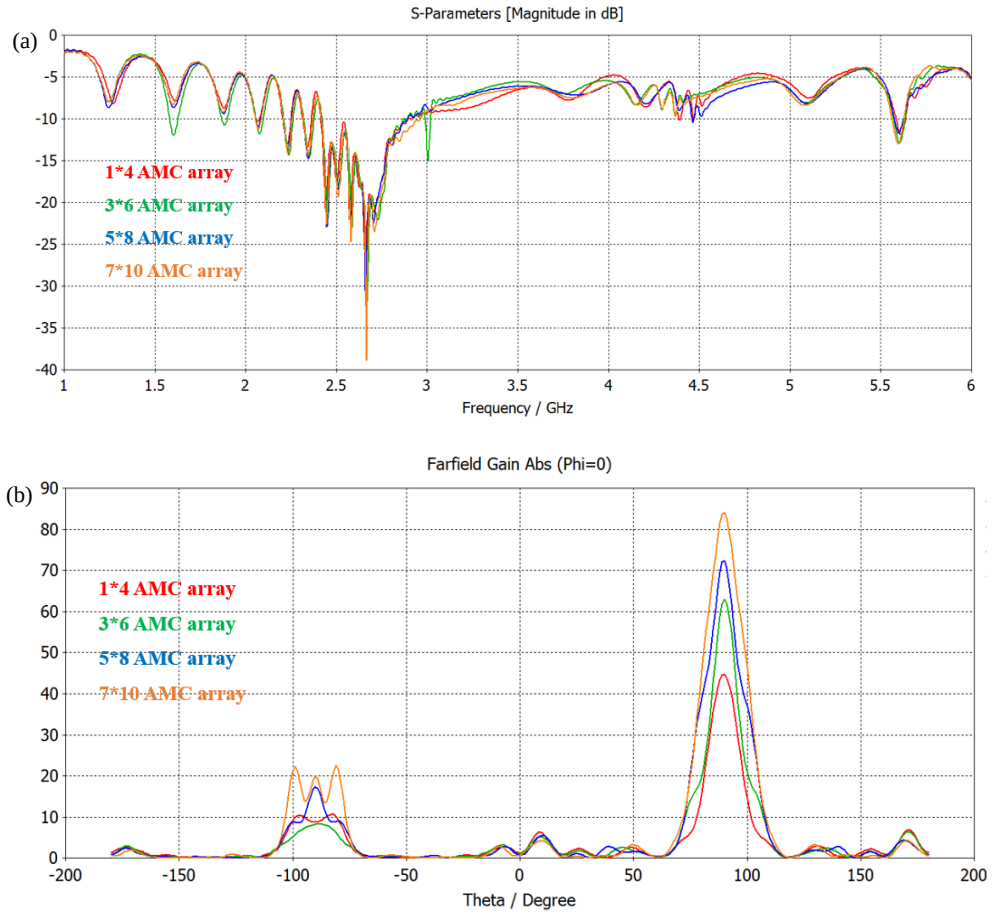

FIGURE 14. AMC array cells influence. (a) S_{11} and (b) far-field gain.

TABLE 1. Hilbert inclusion with AMC structure frequency reconfiguration.

Case	Input sequence	Number of bands	Resonance frequency	4 GHz		5 GHz		5.5 GHz	
				S_{11}	Gain	S_{11}	Gain	S_{11}	Gain
1	1111111111111111	7	3.7, 4, 4.3, 4.4, 4.8, 5.3, 5.7	−8	5	−7	9		
2	11111111000000000	6	3.7, 4.1, 4.3, 5, 5.4, 5.9	−7	6	−12	12	−10	18
3	11111100000000000	6	3.7, 4.1, 4.3, 5, 5.5, 5.9			−12	13	−16	19
4	10101010101010101	6	3.7, 4.1, 4.3, 5, 5.5, 5.8			−11	11	−8	17
5	11100000000000000	5	3.7, 4.1, 4.3, 5, 5.5					−16	20
9	10000000000000000	5	3.7, 4.1, 4.3, 5, 5.6						

TABLE 2. Multi-band frequency response under different PIN diode configurations.

Cases	Input sequence	Number of bands	Resonance frequency
1	1111111111111111	15	0.3, 2.2, 3.1, 3.2, 3.3, 3.4, 3.5, 3.6, 3.7, 4.7, 4.8, 5.2, 5.6, 5.9
2	0000000000000000	14	0.3, 2.2, 3.1, 3.2, 3.3, 3.4, 3.5, 3.6, 3.8, 4, 4.4, 4.7, 5, 5.3
3	11111111000000000	15	0.3, 2.2, 3, 3.1, 3.2, 3.3, 3.4, 3.5, 3.6, 4, 4.4, 4.7, 5, 5.2, 5.3
4	11111100000000000	10	0.3, 2.2, 3.1, 3.2, 3.3, 3.5, 3.6, 3.9, 4.1, 4.5
5	10101010101010101	13	0.3, 2.2, 2.3, 3, 3.1, 3.2, 3.3, 3.4, 3.5, 3.6, 3.7, 4.1, 4.5, 5.5

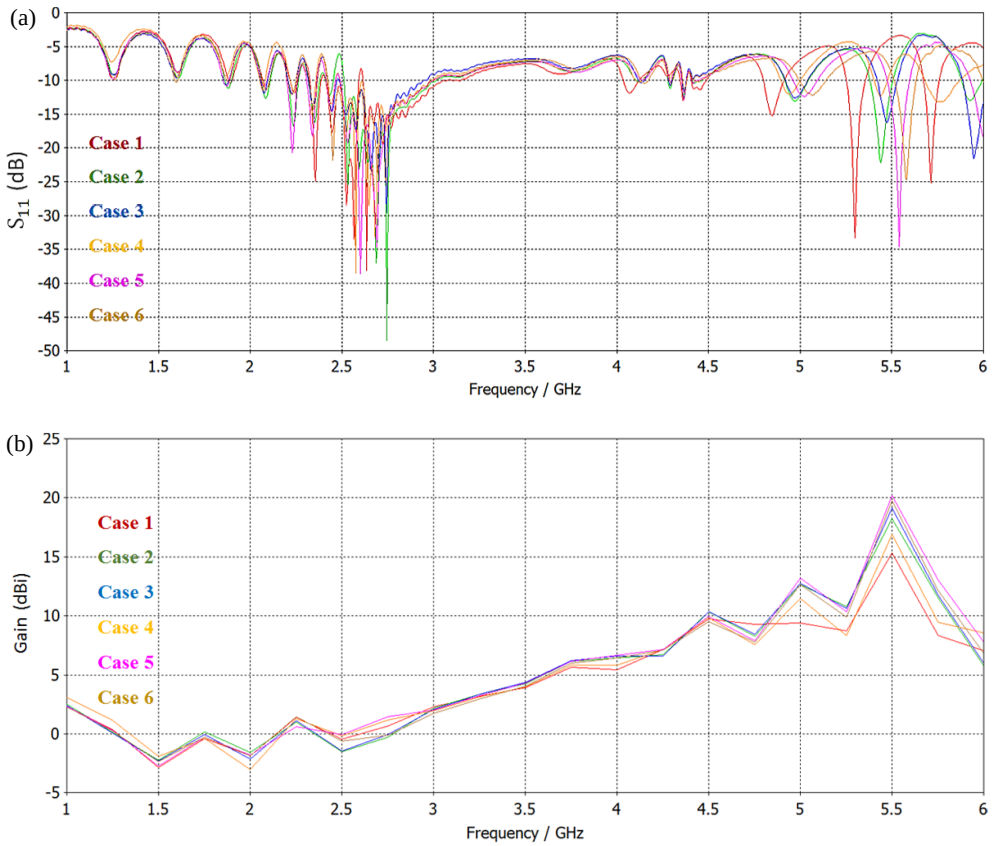

FIGURE 15. AMC reconfiguration. (a) S_{11} and (b) gain.

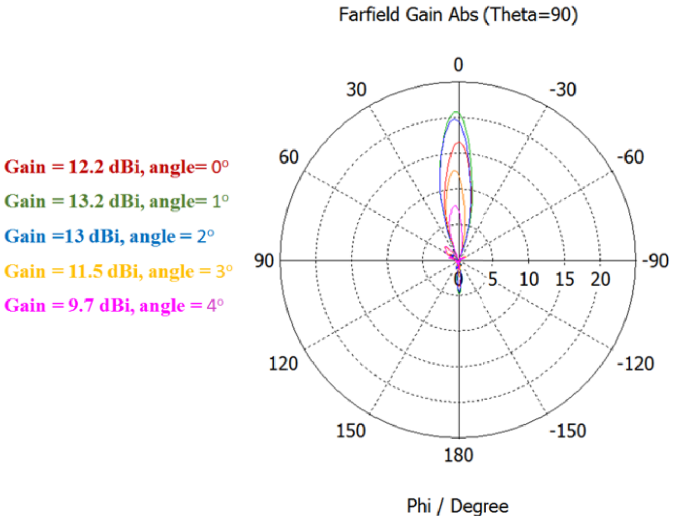

FIGURE 16. The proposed AMC structure beam-scan at 5 GHz.

Figure 15(b) shows the effect of the OS on antenna gain, and changing the OS state affects the surface current distribution, which results in gain control at the same resonance frequency; a peak gain of 20 dBi is achieved at 5.5 GHz.

By changing the OS value, the electrical length and impedance of the CRLH structure are altered, which modifies the phase distribution of the current surface; as a result, a progressive phase variation is introduced which tilts the main radiation in a specific direction. The antenna can scan up to 5° at 5 GHz while maintaining good impedance and consistent gain, which is useful for tracking objects [21], as seen in Figure 16.

4.4. Fabrication and Experimental Validation

An AMC MTS was added to the proposed design to reduce the back lobes and interference. A wet chemical fabrication process was used in the proposed antenna fabrication procedure, whereby the fabricated antenna was introduced during the measurement process. The antenna was installed on a rotating table inside a special radio frequency (RF) chamber and connected to a spectrum analyzer to measure the radiation intensity. A 37347A vector network analyzer was used to measure the antenna parameters.

The measurements are shown in Figures 17(a)–(b). For frequency reconfiguration, visible light was used to lighten the OS through the measurement process. In addition, a black plastic lid covered the OS to ensure full darkness for the case (OFF) during the measurement. To validate the design, two cases were considered, one with the OS switch OFF and one with the OS switch ON. These cases were compared with the CST results without and with the proposed AMC reflector, and the S_{11} and gain spectra are evaluated for each. First, the S_{11} and gain spectra are calculated for the antenna without the proposed AMC; the antenna's resonant frequency changed significantly when the OS was switched ON/OFF.

In addition, the antenna gain varies considerably, as shown in Figures 18(a)–(b). Furthermore, the simulation results agree with the radiation measurements, where the radiation pattern at

FIGURE 17. The measurements. (a) Antenna under test and (b) S_{11} measurements at OFF (cover with black) state with and without a reflector.

5.5 GHz for the antenna without AMC is calculated for the E- and H-planes, as shown in Figure 18(c).

The main beam is directed to the end-fire direction. The obtained results in terms of S_{11} and radiation pattern are evaluated for the proposed antenna with AMC for ON/OFF states; the simulation results agree with the measurements, as seen in Figures 19(a)–(b), for S_{11} spectra. The antenna radiation patterns are presented in Figure 19(c) for both cases; excellent agreement is achieved between the simulated and measured results.

To further validate the proposed design, a quantitative comparison between simulated and measured results is presented. At 5.5 GHz, the measured gain is approximately 19.2 dBi compared to 20 dBi in simulation, resulting in a deviation of about 4%. Similarly, the measured S_{11} shows a slight frequency shift of approximately 1.8%, which can be attributed to fabrication tolerances, SMA connector losses, and dielectric constant variations. These small deviations confirm the robustness and practical feasibility of the proposed antenna design. The radiation efficiency of the proposed antenna is estimated to be higher than 85% across the operating band, which indicates that the integration of the proposed AMC reflector and LDR switching mechanism does not significantly degrade antenna performance. It is important to note that the proposed antenna is primarily intended for high-gain applications, such as base stations and directional communication systems, where size constraints are less critical than performance requirements.

5. COMPARISON WITH MOST RECENT RESULTS OF INTEREST

Table 3 summarizes a comparison with the most recent literature. The proposed design provides a higher gain than the other designs, in addition to the ability for beam scan, gain control, and frequency reconfiguration.

The significant gain improvement achieved by the proposed antenna compared to the designs in Table 3 is due to a combination of integrated electromagnetic factors. The 17-cell CRLH array provides a larger effective radiating area, resulting in increased directionality. Furthermore, the use of a Hilbert structure instead of conventional vias reduces conduction losses and surface-wave propagation, positively impacting radiating efficiency. Additionally, the proposed AMC reflector provides near-zero phase reflection at the operating frequency, generating constructive interference that redirects the radiated power in the forward direction. The proposed structure also contributes to a more uniform distribution of current and electro-

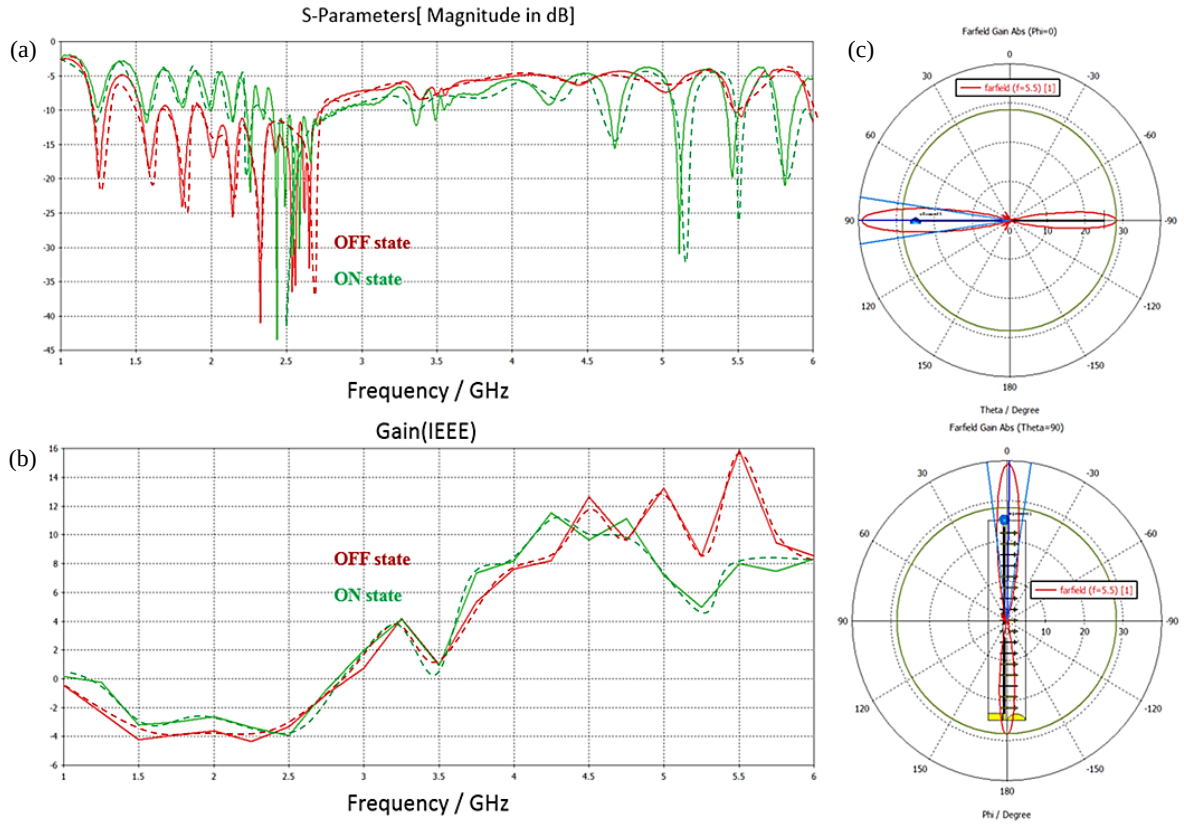

FIGURE 18. The validation comparison without AMC. (a) S_{11}, (b) gain, noted that solid lines for simulation and dotted lines for measurements, and (c) radiation patterns.

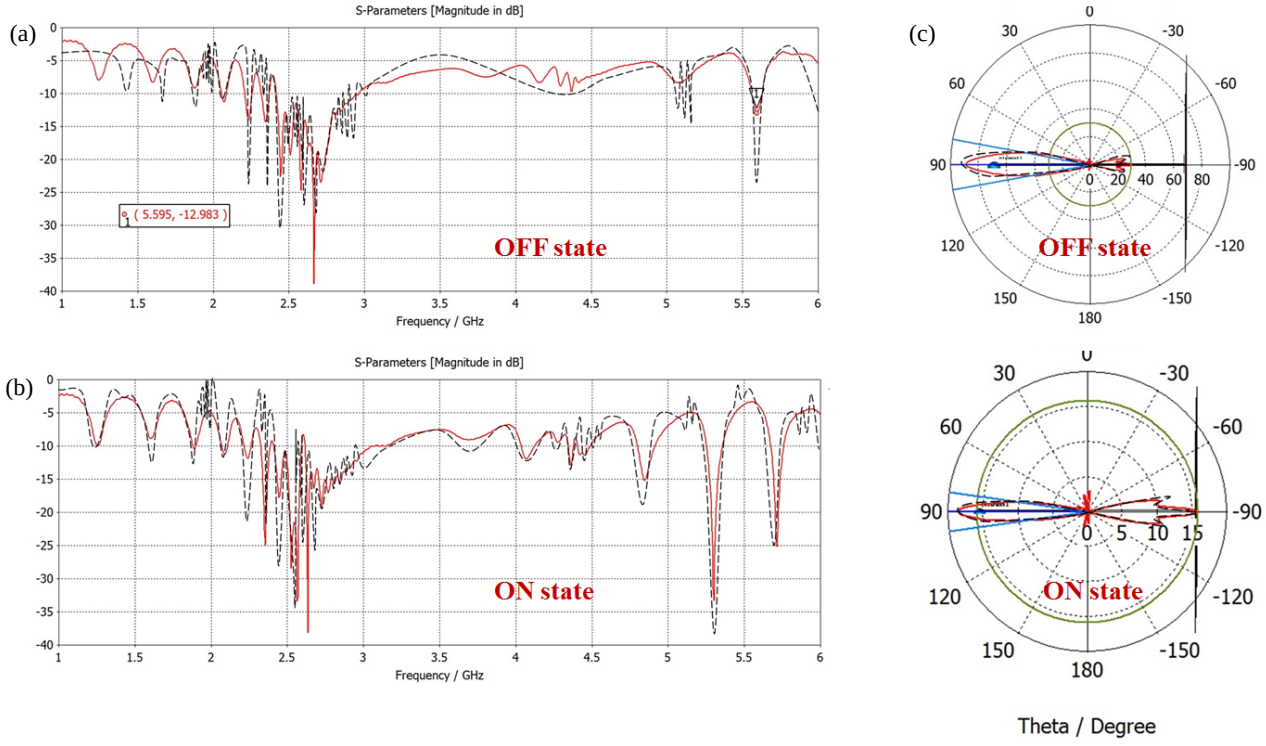

FIGURE 19. The validation comparison with AMC. (a) S_{11} at OFF state, (b) S_{11} at ON state, noted that solid lines for simulation and dotted lines for measurements, and (c) radiation patterns.

TABLE 3. The comparison of the proposed AMC reflector antenna with most recent results of interest.

Ref.	Size	Bandwidth GHz	Reconfigurable	Technique used	Frequency	Max. gain	Via	Substrate
[22]	127 × 200 × 16.2	3.28–5.31	No	Slots patch + AMC	3.26–3.73, 4.68–5.05	15.7	12	F4B
[23]	30 × 50	4.8–6.7	No	Planar inverted-F antenna + AMC	4.8–6.7	7.6	—	RT 5880
[24]	79.7 × 79.7 × 11.1	3.14–3.83	No	Bowtie dipoles + AMC	3.1–3.8, 4.4–5	8.2	2	FR-4
[25]	64 × 64 × 17.2	-	No	Monopole + AMC	2.38–2.7, 3.28–5.8	7.1	—	FR-4
[26]	32.8 × 32.8 × 6.8	4.25–7.10	No	Dipole + AMC	4.48–7	8.2	1	FR-4
[27]	90 × 90 × 15.75	2.91 to 5.6	Yes	Monopole + AMC	3–5.09	8.7	—	R 4003C
[28]	-	4.90 to 6.70	No	Slotted a bow-tie antenna + AMC	2.4–2.7, 3.4–3.8, 5.17–6.45	10.5	—	Arlon 880
[29]	280 × 280	1.8–5.4	Yes	Metasurface + PIN diodes (frequency & pattern reconfiguration)	1.8/2.7/3.1/3.3/ 4.1/5.1/5.4	11.1	—	Taconic FR-30
[30]	108 × 108	0.1–0.3	No	Metamaterial superstrate + U-shape patch	2.6/4.2/5.6	8.04	—	Taconic FR-30
[31]	60 × 60 × 6.8	3.26–6.05	No	Dipole + AMC	3.26–6.02	8.4	—	Taconic TLT
[32]	22 × 22 × 1.6		No	Slots-patches + AMC	1.7–2.5, 5.1–5.6	7.2	—	FR4
Proposed design	179 × 123	5.51–5.66	Yes	CRLH + Hilbert + AMC	5.51–5.66	20	—	Taconic RF-43

magnetic fields, thereby reducing unwanted field cancellation and achieving a high gain of up to 20 dBi.

6. CONCLUSION

A CRLH antenna with a zero-phase AMC reflector is introduced to achieve a high gain-bandwidth product for 5G-sub 6 GHz applications. First, an array of 1×17 CRLH unit cells coupled to a third-order Hilbert curve structure to reduce surface waves was designed and tested. The antenna provided a high gain of 16 dBi at 5.6 GHz; however, the design suffered from high back lobes. Thus, introducing the in-phase AMC reflector on the backside of the selected design reflects the back lobe with zero phase in the interested band, resulting in a high-gain (20 dBi) unidirectional pattern. Frequency reconfiguration and beam steering can be accomplished through an OS placed in the T-section CRLH unit cell. By activating/deactivating the OS, various bands with high gain can be achieved, using a free wire biasing system without any mechanical effort or complicated electrical biasing systems. The antenna can scan up to $\pm 5^{\circ}$ with a consistent gain. In addition, the DAM can be obtained for the proposed designs by varying the OS to create various levels of transmission states. The measurement results confirm the validity and accuracy of the proposed design. Future work will focus on further miniaturization of the antenna by optimizing the proposed AMC structure and employing compact metamaterial configurations.

REFERENCES

[1] Elwi, T. A., F. Taher, B. S. Virdee, M. Alibakhshikenari, I. J. G. Zuazola, A. Krasniqi, A. S. Kamel, N. T. Tokan, S. Khan, N. O. Parchin, *et al.*, "On the performance of a photonic reconfigurable electromagnetic band gap antenna array for 5G applications," *IEEE Access*, Vol. 12, 60 849–60 862, 2024.

[2] Elwi, T. A., H. H. Al-Khaylani, W. S. Rasheed, S. A. Al-Salim, M. H. Khalil, L. A. Ali, O. A. Tawfeeq, S. T. Al-Hadeethi, D. Ali, Z. S. Muqdad, S. Özbay, and M. M. Ismael, "On the performance of metamaterial based printed circuit antenna for blood glucose level sensing applications: A case study," *Infocommunications Journal*, Vol. 16, No. 1, 56–63, Mar. 2024.

[3] Majeed, A. M., T. A. Elwi, Z. A. A. Hassain, J. Kumar, and A. E. Saleem, "Orbital angular momentum-based slot array antenna for modern applications," *Journal of Engineering and Sustainable Development*, Vol. 28, No. 3, 375–383, 2024.

[4] Al-Saegh, A. M., F. Taher, T. A. Elwi, M. Alibakhshikenari, B. S. Virdee, O. Abdullah, S. Khan, P. Livreri, A. Al-Jumaily, M. F. A. Sree, *et al.*, "AI-based investigation and mitigation of rain effect on channel performance with aid of a novel 3D slot array antenna design for high throughput satellite system," *IEEE Access*, Vol. 12, 29 926–29 939, 2024.

[5] Al-Adhami, A., Y. Al-Adhami, and T. A. Elwi, "A 3D antenna array based solar cell integration for modern MIMO systems," *Infocommunications Journal*, Vol. 15, No. 4, 10–16, 2023.

[6] Jwair, M. H., T. A. Elwi, S. K. Khamas, A. Farajidavar, and A. B. Ismail, "Circularly shaped metamaterial fractal reconfigurable antenna for 5G networks," *Iraqi Journal of Information*

and Communication Technology, Vol. 6, No. 3, 65–75, 2023.

[7] Abood, M. S., H. Wang, D. He, M. Fathy, S. A. Rashid, M. Alibakhshikenari, B. S. Virdee, S. Khan, G. Pau, I. Dayoub, P. Livreri, and T. A. Elwi, "An LSTM-based network slicing classification future predictive framework for optimized resource allocation in C-V2X," *IEEE Access*, Vol. 11, 129 300–129 310, 2023.

[8] Abdulsattar, R. K., S. M. Sadeq, T. A. Elwi, Z. A. A. Hassain, and M. Y. Muhsin, "Artificial neural network approach for estimation of moisture content in crude oil by using a microwave sensor," *International Journal of Microwave & Optical Technology*, Vol. 18, No. 5, 511–519, 2023.

[9] Jwair, M. H., T. A. Elwi, M. Alibakhshikenari, B. S. Virdee, H. Almizan, Z. A. A. Hassain, S. M. Ali, L. Kouhalvandi, P. Livreri, N. T. Tokan, *et al.*, "Intelligent metasurface layer for direct antenna amplitude modulation scheme," *IEEE Access*, Vol. 11, 77 506–77 517, 2023.

[10] Ismail, M. M., T. A. Elwi, and A. J. Salim, "Design and simulation of a CRLH transmission line antenna of a Hilbert fractal geometry for S-band appications," in *2021 International Conference on Electrical, Computer and Energy Technologies (ICECET)*, 1–5, Cape Town, South Africa, 2021.

[11] Hussein, H., F. Atasoy, and T. Elwi, "Origami antenna array shaped mosque of Muhammed Al-Fatih for visual sight enhancement in modren 5G MIMO networks," *Journal of Engineering and Sustainable Development*, Vol. 27, No. 4, 417–428, 2023.

[12] Ali, L., M. Ilyas, and T. A. Elwi, "A metamaterial-based compact MIMO antenna array incorporating Hilbert fractal design for enhanced 5G wireless communication networks," *Mathematical Modelling of Engineering Problems*, Vol. 10, No. 3, 930–936, 2023.

[13] Al Naiemy, Y., R. Gaib, R. K. Abdulsattar, Z. S. Muqdad, T. A. Oleiwi, and A. H. Mohammed, "Optimizing resource allocation in RIS-assisted MIMO systems using deep Q-learning," in *2025 5th International Conference on Artificial Intelligence and Signal Processing (AISP)*, 1–5, Vijayawada, India, 2025.

[14] Al-Attar, S., M. Alibakhshikenari, Y. M. Qasaymeh, *et al.*, "A reconfigurable MTM-EMBG MIMO antenna array with solar panel integration for sustainable 5G networks," *Scientific Reports*, 2026.

[15] Jwair, M. H. and T. A. Elwi, "Metasurface antenna circuitry for 5G communication networks," *Infocommunications Journal: A Publication of the Scientific Association for Infocommunications (HTE)*, Vol. 15, No. 2, 2–7, 2023.

[16] Alibakhshikenari, M., B. S. Virdee, T. A. Elwi, I. D. Lubangakene, R. K. R. Jayanthi, A. A. Al-Behadili, Z. A. A. Hassain, S. M. Ali, G. Pau, P. Livreri, and S. Aïssa, "Design of a planar sensor based on split-ring resonators for non-invasive permittivity measurement," *Sensors*, Vol. 23, No. 11, 5306, 2023.

[17] Abdulsattar, R. K., M. Alibakhshikenari, B. S. Virdee, R. Sharma, T. A. Elwi, L. Kouhalvandi, Z. A. A. Hassain, S. M. Ali, N. T. Tokan, P. Livreri, F. Falcone, and E. Limiti, "Optical-microwave sensor for real-time measurement of water contamination in oil derivatives," *AEU — International Journal of Electronics and Communications*, Vol. 170, 154798, 2023.

[18] Hussein, H., F. Atasoy, and T. A. Elwi, "Miniaturized antenna array-based novel metamaterial technology for reconfigurable MIMO systems," *Sensors*, Vol. 23, No. 13, 5871, 2023.

[19] Al Naiemy, Y., M. Q. Abdalrazak, Z. S. Muqdad, R. K. Abdulsattar, T. A. Oleiwi, and R. Al-Shabandar, "On the performance of RIS systems for modern communication networks," in *2025 5th International Conference on Artificial Intelligence and Signal Processing (AISP)*, 1–5, Vijayawada, India, 2025.

[20] Abbood, H. T., B. Ünal, and T. A. Oleiwi, "A dual band rectenna designed with binary coding technique of genetic algorithm," in *2025 5th International Conference on Artificial Intelligence and Signal Processing (AISP)*, 1–6, Vijayawada, India, 2025.

[21] Alnaiemy, Y., M. Q. Abdalrazak, Z. Salam, and T. A. Elwi, "On the performance of CRLH antenna loaded with AMC reflector for direct antenna modulation process," *Progress In Electromagnetics Research C*, Vol. 166, 244–256, 2026.

[22] Al-Asady, R., T. A. Elwi, and B. Ruthramurthy, "A modern RIS design based AI driven for cooperative relay networks," *Iraqi Journal of Information and Communication Technology*, Vol. 8, No. 3, 73–82, 2025.

[23] Ali, M. M., E. M. Segura, and T. A. Elwi, "High-gain CRLH Vivaldi antenna for enhanced channel performance at Ku-band communication systems," *Scientific Reports*, Vol. 16, No. 1, 8651, 2026.

[24] Liu, Q., H. Liu, W. He, and S. He, "A low-profile dual-band dual-polarized antenna with an AMC reflector for 5G communications," *IEEE Access*, Vol. 8, 24 072–24 080, 2020.

[25] Ashish, J. and A. P. Rao, "A dual band AMC backed antenna for WLAN, WiMAX and 5G wireless applications," *Applied Computational Electromagnetics Society Journal (ACES)*, Vol. 36, No. 9, 1209–1214, 2021.

[26] Malekpoor, H., A. Abolmasoumi, and M. Hamidkhani, "High gain, high isolation, and low-profile two-element MIMO array loaded by the Giuseppe Peano AMC reflector for wireless communication systems," *IET Microwaves, Antennas & Propagation*, Vol. 16, No. 1, 46–61, 2022.

[27] Askari, H., N. Hussain, D. Choi, M. A. Sufian, A. Abbas, and N. Kim, "An AMC-based circularly polarized antenna for 5G sub-6 GHz communications," *Computers, Materials, & Continua*, Vol. 69, No. 3, 2997–3013, 2021.

[28] De Mello, R. G. L., A. C. Lepage, and X. Begaud, "A low-profile, triple-band, and wideband antenna using dual-band AMC," *Sensors*, Vol. 23, No. 4, 1920, 2023.

[29] Elias, B. Q., M. M. Ismail, B. S. Bashar, A. I. Alanssari, Z. A. Rhazali, and H. Misran, "Multi-beam metasurface control based on frequency reconfigurable antenna," *Informacije MIDEM*, Vol. 54, No. 2, 77–85, 2024.

[30] Elwi, T. A., Z. A. Rhazali, H. Misran, M. M. Ismael, B. B. Q. Elias, *et al.*, "A beam-split and gain-enhanced patch antenna using metamaterial superstrate for wireless communications," *Informacije MIDEM*, Vol. 55, No. 3, 2025.

[31] Malekpoor, H., "AMC-loaded low-profile broadband printed 2×2 array with gain and isolation enhancement using equivalent circuit model for wireless systems," *IEEE Access*, Vol. 11, 22 007–22 017, 2023.

[32] Rajavel, V. and D. Ghoshal, "AMC-based low-profile dual-band slotted patch antenna for IoT devices in the healthcare system," *Iranian Journal of Science and Technology, Transactions of Electrical Engineering*, Vol. 47, No. 2, 437–450, 2023.